

# Conditions for fully gapped topological superconductivity in topological insulator nanowires

Fernando de Juan<sup>1,2,3\*</sup>, Jens H. Bardarson<sup>4</sup>, Roni Ilan<sup>5</sup>

**1** Rudolf Peierls Centre for Theoretical Physics, Oxford University, Oxford, OX1 3PU, United Kingdom

**2** Donostia International Physics Center, P. Manuel de Lardizabal 4, 20018 Donostia-San Sebastian, Spain

**3** IKERBASQUE, Basque Foundation for Science, Maria Diaz de Haro 3, 48013 Bilbao, Spain

**4** Department of Physics, KTH Royal Institute of Technology, Stockholm 10691, Sweden

**5** Raymond and Beverly Sackler School of Physics and Astronomy, Tel-Aviv University, Tel-Aviv 69978, Israel

\* fernando.dejuan@dipc.org

June 10, 2022

## Abstract

Among the different platforms to engineer Majorana fermions in one-dimensional topological superconductors, topological insulator nanowires remain a promising option. Threading an odd number of flux quanta through these wires induces an odd number of surface channels, which can then be gapped with proximity induced pairing. Because of the flux and depending on energetics, the phase of this surface pairing may or may not wind around the wire in the form of a vortex. Here we show that for wires with discrete rotational symmetry, this vortex is necessary to produce a fully gapped topological superconductor with localized Majorana end states. Without a vortex the proximitized wire remains gapless, and it is only if the symmetry is broken by disorder that a gap develops, which is much smaller than the one obtained with a vortex. These results are explained with the help of a continuum model and validated numerically with a tight binding model, and highlight the benefit of a vortex for reliable use of Majorana fermions in this platform.

---

## Contents

<b>1</b>	<b>Introduction</b>	<b>2</b>
<b>2</b>	<b>Continuum model for TI nanowire surface states</b>	<b>4</b>
2.1	Superconductivity in the continuum model	5
2.2	Computation of topological invariant	6
2.3	Phase diagrams from continuum model	8
<b>3</b>	<b>Topological superconductivity in a tight binding model</b>	<b>9</b>

3.1	Phase diagrams	11
<b>4</b>	<b>Discussion and conclusions</b>	<b>12</b>
<b>5</b>	<b>Appendix</b>	<b>14</b>
5.1	Dirac equation in curved space	14
5.2	Effective Hamiltonian with superconductivity	17
5.3	Time reversal symmetry in the continuum model	18
5.4	Transfer matrix method	18
	<b>References</b>	<b>20</b>

---

## 1 Introduction

The physical realization and manipulation of non-Abelian anyons, exotic quasiparticles with neither fermionic nor bosonic statistics, has remained a challenging endeavor in condensed matter physics for decades [1]. Their search continues motivated both by the fundamental aim of discovering new phases of matter and by promising applications in topological quantum computation. The simplest of these quasiparticles, localized Majorana bound states, can appear in defects or on boundaries of topological superconductors [2–5]. These systems are however rare because they require unconventional pairing, but the more recent realization that they can be engineered artificially from more standard components has triggered a renewed effort to find them.

Currently, the most developed proposals are based on one dimensional (1D) superconductors which host Majorana bound states at their ends [6–8], engineered by coupling a metallic 1D system with an odd number of channels at the Fermi level with a superconductor via the proximity effect [9]. The realization of this proposal with semiconductor wires has provided compelling experimental evidence of Majorana bound states (see Ref. [10] and references therein), but several alternative realizations remain promising as well [11–13].

One particularly interesting system that remains relatively unexplored is based on three dimensional topological insulator (TI) nanowires. When the Fermi level lies in the bulk gap, the only transport modes are those derived from the topological surface Dirac fermion [14, 15] which wraps around the surface of the wire. When half of a flux quantum is threaded through the wire cross section, there is an odd number of modes at the Fermi level for any value of the chemical potential, and one of them is perfectly transmitted in the presence of time-reversal symmetry [16–22]. These wires were proposed to realize a topological superconductor in the presence of proximity effect [23, 24] and this proposal has been since studied extensively [25–28]. In particular, the advantages of TI nanowires to build a Majorana qubit architecture for quantum computation were emphasized in a recent proposal [29]. Experimentally, TI nanowires have been realized in several compounds [30–38], where Aharonov-Bohm oscillations of the conductivity reveal that good surface transport has been achieved. The recent observation of Andreev reflection from the surface modes in a nanowire Josephson junction made with TI BiSbSeTe<sub>2</sub> [39, 40] further supports the idea that topological superconductivity

in this system should be within reach.

A key aspect of the proximity effect in wires is that the induced pairing field may acquire an azimuthal phase dependence when the magnetic field is applied, as illustrated in Fig. 1. If the intrinsic superconductor surrounds the wire as in Fig. 1(a), an azimuthal supercurrent will develop upon flux threading, with a tendency to screen the applied flux. As the flux increases, it will become energetically favorable to switch to a state with an azimuthal vortex in the order parameter and no supercurrent, which should be most stable for an applied flux of  $h/2e$ . The proximity induced pairing will naturally inherit this phase profile. However, if the intrinsic superconductor is a thin film contacting one face of the wire as in Fig. 1(b), in the simplest approximation the phase profile of the order parameter and induced pairing field may be assumed constant at any flux. In a realistic setup, the vortex may or may not be present depending on flux, the device, and on material details, and the impact of the vortex on the resulting proximitized state is not sufficiently understood.

As emphasized in Ref. [26], the low energy surface Dirac model necessarily predicts that the vortex is required to produce a topological superconductor. This is because at any finite flux, the lowest energy electron mode has angular momentum of  $l = 1/2$  and simply cannot be gapped out with its hole partner of  $l = -1/2$  if the pairing field is constant and angular momentum is conserved. The vortex is required to compensate the mismatch in angular momentum and open a gap. In the absence of a vortex, the spectrum remains gapless and localized Majorana bound states cannot be defined. This conclusion is at odds with bulk tight binding simulations, which predict that a gapped state can be achieved without a vortex [24]. Another work with a more realistic account of the proximity effect observed both gapped and gapless regions in the absence of the vortex [27]. A better understanding of this problem is thus clearly needed.

In this work, we show with both a low energy model and tight binding calculations that in the presence of any rotation axis  $C_n$  parallel to the field, which requires angular momentum conservation modulo  $n$ , the superconducting state without a vortex must indeed be either trivial or gapless, regardless of the proximity induced pairing strength. We then show how breaking the rotation symmetry may still lead to a gapped topological state in the absence of a vortex. However, the gap magnitude in this case is determined by the symmetry breaking mechanism and is generally much smaller than the magnitude of the pairing strength. In the presence of a vortex, on the contrary, the gap remains of the order of the pairing strength, so the topological superconducting phase is in practice much more robust in this case. We illustrate these points in detail by computing phase diagrams of the gaps and topological phase transitions for several types of wires and pairing potentials, also taking into account the effect of disorder.

The rest of this work is organized as follows. In Sec. 2 we describe the surface effective model from which all our main conclusions can be derived. In Sec. 3 we confirm these results with a lattice tight binding model with proximity effect, considering a number of scenarios. Finally in Sec. 4 we discuss our results and present some conclusions. Several technical derivations are left for the Appendix.

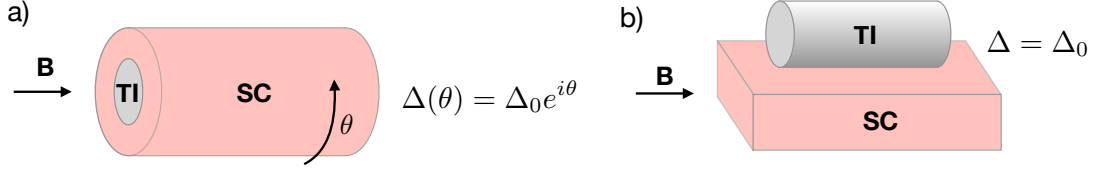


Figure 1: Two simplified setups used to induce the proximity effect in wires in the presence of a magnetic field. In a), the wire is surrounded by a superconducting cylinder, which must itself host a vortex when the flux is  $h/2e$ . The TI then inherits the vortex profile in proximity-induced pairing field. In b), the wire is only partially contacted by the bulk superconductor. In the limit where the superconductor is a thin film no vortices are expected, and the induced pairing in the wire will be approximately constant.

## 2 Continuum model for TI nanowire surface states

Topological insulators are guaranteed to possess a Dirac fermion surface state [14] which dominates their transport properties when the chemical potential  $\mu$  is in the bulk band gap. The appropriate low energy model to describe this surface state is a Dirac Hamiltonian in the corresponding surface geometry [16–18, 24, 26]. To discuss superconductivity in wires, we consider a cylindrical sample of radius  $R$  and cross section  $A = \pi R^2$  oriented along the  $x$  direction. The surface of the wire is parametrized in cylindrical coordinates  $(x, \theta)$ . The wire is in the presence of a magnetic field  $\vec{B} = (B_{\parallel}, 0, 0)$  which threads a dimensionless flux  $\eta = B_{\parallel}A/(h/e)$  through the cross section. The magnetic field is described with the vector potential  $\vec{A} = B_{\parallel}(0, -z/2, y/2)$ , so that translational invariance is preserved in the  $x$  direction. The effect of the Zeeman coupling is not essential and will be discussed in Sec. 4. The effective Dirac equation for the surface states is  $H\psi = E\psi$  with Hamiltonian

$$H = -i\sigma_x\partial_x + \frac{1}{R}\sigma_y(-i\partial_\theta + \eta), \quad (1)$$

where we set  $\hbar = 1$  and the Fermi velocity  $v_F = 1$ . In these units,  $1/R$  is the natural energy unit for the problem. The wave functions satisfy antiperiodic boundary conditions in  $\theta$  due to the curvature-induced  $\pi$  Berry phase [17, 18]. There are several ways to derive this Hamiltonian [16–18, 24, 26], which are summarized in Appendix 5.1. This model has an effective full rotational symmetry around the wire axis  $\theta \rightarrow \theta + \theta'$  for any  $\theta'$ .

The Hamiltonian can be diagonalized by Fourier transforming the spinor  $\psi(x, \theta) = \int dx \sum_n e^{ikx} e^{il\theta} \psi_{k,l}$ , where  $l$  is half-integer,  $l = \pm\frac{1}{2}, \pm\frac{3}{2}, \dots$ , because of the antiperiodic boundary conditions. The  $l$ -th block of the transformed Hamiltonian is

$$H_l = \sigma_x k + \frac{1}{R}(l - \eta)\sigma_y. \quad (2)$$

When  $\eta = 1/2$ , which corresponds to half of a flux quantum threaded through the wire, the  $l = 1/2$  mode is gapless, linearly dispersing, and perfectly transmitted [20], while the rest of the modes are doubly degenerate and gapped.

## 2.1 Superconductivity in the continuum model

Since  $l = 1/2$  is the only non-degenerate mode at  $\eta = 1/2$ , the number of channels is odd for any chemical potential, and including superconducting pairing through the proximity effect should result in a topological superconductor according to Kitaev [9], as long as the resulting spectrum becomes gapped by the pairing. To see whether the spectrum becomes gapped we model superconductivity with a BdG Hamiltonian  $\mathcal{H} = \frac{1}{2}\Psi^\dagger H \Psi$  written in terms of Nambu spinors  $\Psi = \begin{pmatrix} \psi \\ -i\sigma_y(\psi^\dagger)^T \end{pmatrix}$  and

$$H = [-i\sigma_x\partial_x + \frac{1}{R}\sigma_y(-i\partial_\theta + \eta\tau_z) - \mu] \tau_z + \tau_x\text{Re}[\Delta(x, \theta)] + \tau_y\text{Im}[\Delta(x, \theta)], \quad (3)$$

where  $\tau_i$  are Pauli matrices in the Nambu space (see Appendix 5.2). By the BdG construction, this Hamiltonian has a particle-hole symmetry  $H = -U_C H^* U_C^\dagger$ , with the unitary part  $U_C = \sigma_y \tau_y$ . The complex pairing function  $\Delta(x, \theta)$  depends on the way the proximity effect is realized. In particular, as discussed in Fig. 1,  $\Delta(x, \theta)$  may have a phase winding around the perimeter of the wire. If the wire is surrounded by a superconducting shell, it is natural that this shell develops a phase winding at certain values of the flux, which is transferred to the induced pairing  $\Delta(x, \theta) = \Delta_0 e^{in_v\theta}$ , with  $n_v$  the number of vortices. In a more thin film geometry, one may rather expect a roughly homogeneous order parameter which can be approximated by a constant  $\Delta(x, \theta) = \Delta$ , so  $n_v = 0$ .

The subtlety with the gaplessness of superconductivity in this system can now be explained by comparing the  $n_v = 0, 1$  cases. The Fourier transformed Hamiltonian for  $n_v = 0$  and angular momentum  $l$ , denoted as  $H_l^{(0)}$ , is

$$H_l^{(0)} = [\sigma_x k + \frac{1}{R}(l - \eta\tau_z)\sigma_y - \mu] \tau_z + \tau_x \Delta_0, \quad (4)$$

with  $l = \pm\frac{1}{2}, \pm\frac{3}{2}, \dots$ . Note that due to the structure of the Fourier transform, particle-hole symmetry takes the form  $H_l(k) = -U_C^\dagger H_{-l}^*(-k) U_C$ , i.e., it reverses angular momentum. For  $n_v = 1$  we have

$$H^{(1)} = [-i\sigma_x\partial_x + \frac{1}{R}\sigma_y(-i\partial_\theta + \eta\tau_z) - \mu] \tau_z + (\tau_x \cos\theta + \tau_y \sin\theta)\Delta_0. \quad (5)$$

Rotational invariance appears to be broken by the pairing term, but is explicitly recovered after the gauge transformation  $\Psi \rightarrow e^{-i\tau_z\theta/2}\Psi$  which results in the Hamiltonian

$$H^{(1)} = [-i\sigma_x\partial_x + \frac{1}{R}\sigma_y(-i\partial_\theta + (\eta - \frac{1}{2})\tau_z) - \mu] \tau_z + \tau_x \Delta_0. \quad (6)$$

Crucially, this transformation also changes the boundary conditions back to periodic, so using the same Fourier transform we get

$$H_l^{(1)} = [\sigma_x k + \frac{1}{R}(l - (\eta - \frac{1}{2})\tau_z)\sigma_y - \mu] \tau_z + \tau_x \Delta_0, \quad (7)$$

where now angular momenta take integer values  $l = 0, \pm 1, \dots$

When  $\Delta_0 = 0$ , the Hamiltonians for  $n_v = 0$  and  $n_v = 1$  give identical spectra as expected. An example spectra for  $\eta = 1/2$ , for a chemical potential where only the first mode is occupied is shown in Fig. 2(a). When pairing is included, however, the spectra are markedly different. For  $n_v = 0$  the spectrum remains gapless, because the electron branch at the Fermi level has  $l = 1/2$ , while the hole branch has a different angular momentum  $l = -1/2$ , and different angular momentum sub-blocks in the Hamiltonian cannot be mixed by the constant pairing,

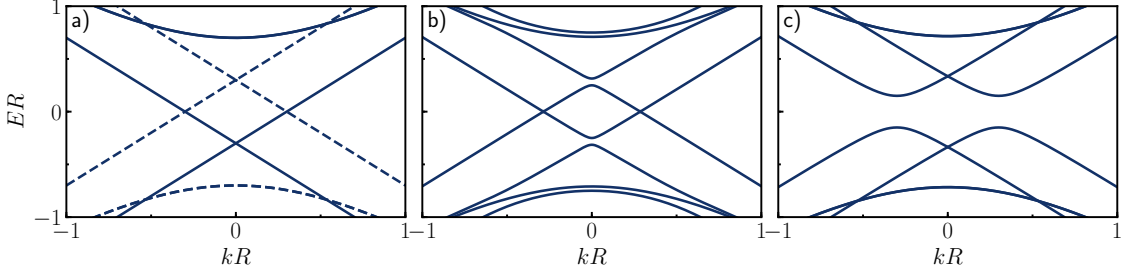


Figure 2: Spectra of topological insulator nanowires obtained from the effective Hamiltonians in Eqs. (4) and (7) with  $\mu R = 0.3$ , when a flux of  $\eta = 1/2$  is applied. a) In the absence of pairing,  $\Delta_0 R = 0$ , the spectrum is gapless with an odd number of modes at any  $E$ . Electron and hole modes are shown with full and dashed lines, respectively. b) In the presence of a pairing field without a vortex, the spectrum remains gapless due to angular momentum conservation. c) In the presence of a vortex, the spectrum becomes gapped. In b) and c)  $\Delta_0 R = 0.15$ .

which preserves rotation symmetry. This is shown in Fig. 2(b). For  $n_v = 1$ , however, electron and hole branches at the Fermi level are particle-hole conjugates of  $l = 0$ , and the pairing can gap them out, as shown in Fig. 2(c). In essence, the vortex has provided the extra unit of angular momentum to compensate the mismatch. The first conclusion of the effective model is thus clear: a vortex is needed for superconductivity to gap out the system at  $\eta = 1/2$ .

## 2.2 Computation of topological invariant

We now determine whether each of the Hamiltonians for  $n_v = 0, 1$  is in a topological phase or not, featuring Majorana edge modes in open geometries. This can be done by computing the topological invariant  $\nu$  defined by Kitaev [9], sometimes called the Kitaev or Majorana number. This invariant is formally defined only for lattice systems with a full gap throughout the Brillouin Zone, and can be computed from the Hamiltonian matrix in the following way. First, a unitary transformation is used to express the Hamiltonian in the basis where particle-hole symmetry operation takes the simple form  $H(k) = -H^*(-k)$ , known as the Majorana basis. In this basis,  $H$  is purely imaginary and antisymmetric at the particle-hole invariant momenta  $k = 0$  and  $k = \pi$ . The invariant is then computed as the product of Pfaffians

$$\nu = \text{sign} [\text{Pf}[iH(0)]\text{Pf}[iH(\pi)]] . \quad (8)$$

This invariant can only change when there is a gap closing at either  $k = 0$  or  $k = \pi$ . The continuum model for the surface states of a TI nanowire assumes that any bands at  $k = \pi$  are far away in energy and are never involved in superconductivity, and therefore changes in the topological invariant can be tracked by computing the Pfaffian at  $k = 0$ , which we now compute. For any particle-hole invariant block diagonal Hamiltonian, the Pfaffian can be decomposed as the product of the Pfaffians for each block. Starting with the case without a vortex, the Hamiltonian in Eq. (4) is block diagonal in angular momentum  $l$ , but particle hole symmetry maps blocks with angular momentum  $\pm l$  into each other, so the smallest block to compute the Pfaffian must include both  $\pm l$  subblocks. Defining Pauli matrices  $\alpha_i$  that act

on this degree of freedom, a doubled Hamiltonian for a given  $|l|$  can be written as

$$H_{|l|} = \left[ \sigma_x k + \frac{1}{R}(l\alpha_z - \eta\tau_z)\sigma_y - \mu \right] \tau_z + \tau_x \Delta_0 \quad (9)$$

and particle-hole symmetry is implemented as  $H_{|l|}(k) = -U_C H_{|l|}^*(-k) U_C^\dagger$  with  $U_C = \sigma_y \tau_y \alpha_x$ . To switch to the Majorana basis, we employ a unitary transformation  $H^M = U_M H U_M^\dagger$  constructed such that  $U_M U_C U_M^T = 1$ , so that particle-hole symmetry becomes  $H_{|l|}^M(k) = -H_{|l|}^{M*}(-k)$  as required. This matrix is  $U_M = U \otimes U'$  where  $U$  acts on spin and particle-hole indices and is given by

$$U = \frac{1}{\sqrt{2}} \begin{pmatrix} \mathcal{I} & -i s_y \\ -i \mathcal{I} & s_y \end{pmatrix} \quad (10)$$

and  $U'$  is

$$U' = 1/2[(1+i)\mathcal{I} + (1-i)\alpha_x] \quad (11)$$

In this basis, the Hamiltonian is

$$H_{|l|}^M = \sigma_x k - \frac{1}{R} l \alpha_y \sigma_y \tau_y - \eta \sigma_y + \mu \tau_y + \sigma_y \tau_x \Delta_0. \quad (12)$$

The Pfaffian at  $k = 0$  is

$$\text{Pf}[iH_{|l|}^M(0)] = [\eta^2 - R^2(\Delta_0^2 + \mu^2)]^2 / R^4 + [l^4 - 2l^2(\eta^2 + R^2(-\Delta_0^2 + \mu^2))] / R^4, \quad (13)$$

and the Majorana number is

$$\nu = \text{sign} \left[ \prod_{l=1/2, 3/2, \dots} \text{Pf}[iH_{|l|}^M(0)] \right]. \quad (14)$$

In the case where a vortex is present in the superconducting order parameter, described by the Hamiltonian in Eq. (7),  $l$  is an integer and the  $l = 0$  block has to be considered separately because it transforms into itself under particle-hole symmetry. For  $l \neq 0$  the Hamiltonian and the Pfaffian are the same as before except  $\eta \rightarrow \eta - \frac{1}{2}$  and  $l$  is an integer so

$$H_{|l| \neq 0} = \left[ \sigma_x k + \frac{1}{R}(l\alpha_z - (\eta - \frac{1}{2})\tau_z)\sigma_y - \mu \right] \tau_z + \tau_x \Delta_0 \quad (15)$$

and

$$\begin{aligned} \text{Pf}[iH_{|l| \neq 0}^M(0)] &= [(\eta - 1/2)^2 - R^2(\Delta_0^2 + \mu^2)]^2 / R^4 \\ &+ [l^4 - 2l^2((\eta - 1/2)^2 + R^2(-\Delta_0^2 + \mu^2))] / R^4. \end{aligned} \quad (16)$$

The Hamiltonian for  $l = 0$  is transformed with Eq. (10) alone and gives

$$H_0^M = \sigma_x k - (\eta - 1/2)\sigma_y + \mu \tau_y + \sigma_y \tau_x \Delta_0, \quad (17)$$

and the Pfaffian is

$$\text{Pf}[iH_0^M(k=0)] = -\Delta_0^2 - \mu^2 + (\eta - 1/2)^2 / R^2. \quad (18)$$

The Majorana number is

$$\nu = \text{sign} \left[ \text{Pf}[iH_0^M(0)] \prod_{|l| \neq 0} \text{Pf}[iH_{|l| \neq 0}^M(0)] \right]. \quad (19)$$



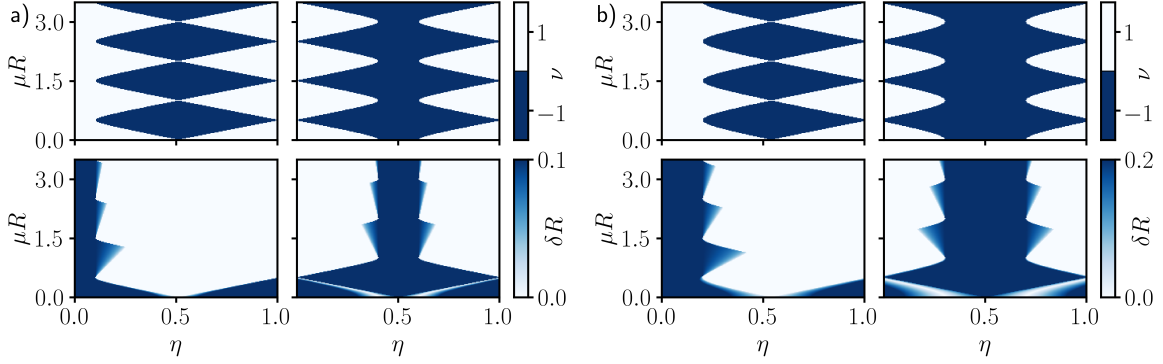


Figure 3: (a) Topological invariant (upper subpanels) and gap estimate  $\delta R$  (lower subpanels) obtained from the continuum model, with a vortex absent (left subpanels) or present (right subpanels). The pairing potential is  $\Delta_0 R = 0.1$ . (b) is the same as a) but with  $\Delta_0 R = 0.2$ .

### 2.3 Phase diagrams from continuum model

With the analytical expressions for the Pfaffian at  $k = 0$ , given in Eq. (14) (with no vortex) and Eq. (19) (with vortex) we can now map out phase diagrams as a function of different model parameters showing the topological and trivial regions. To do this, we note that at the point  $\Delta_0 = \eta = 0$ , the system is a non-superconducting insulator which must have trivial Majorana number. As we move through the phase diagram, the Majorana number will become non-trivial when the Pfaffian at  $k = 0$  changes sign compared to that point.

To address the problem of whether the superconducting state is gapless, it is useful to display phase diagrams showing both the topological invariant and the gap  $\delta$  induced by superconductivity. The numerical computation of the gap is complicated by the fact that it is not efficient to sweep over  $k$  to find the minimum separation between bands above and below zero, especially so once we consider lattice models with many bands in the next section. Because of this, we consider an alternative method to estimate the gap based on the transfer matrix approach, explained in detail in Appendix 5.4, which rather computes the values of the momentum  $k$  for all modes at zero energy (at the Fermi level). Modes that do not cross the Fermi level are evanescent and have a complex momentum  $k = \kappa + i\delta$ , and the imaginary part  $\delta$  for a given mode can be taken as an estimate of its gap (note  $v_F = 1$ ). Numerically, for a given point in the phase diagram we compute  $\delta$  for all modes and take the smallest  $\delta$  as an estimate of the true gap.

With this procedure, we compute phase diagrams as a function of flux  $\eta$  and chemical potential  $\mu$ , which are displayed in Fig. 3 for two values of  $\Delta$ . A first main result is that the topological invariant, taken at face value, is not very different between the cases with and without vortex. This is in agreement with previous work [24]. However, a side by side comparison of the gap and topological invariant clearly shows that, in the absence of a vortex, all regions where the topological invariant is formally nontrivial are in fact gapless. It is only when the vortex is present that a region centered around  $\eta = 1/2$  appears in the phase diagram which has both a nontrivial Majorana number and a finite gap.



### 3 Topological superconductivity in a tight binding model

The results presented in the previous section are ultimately rooted on the full rotational invariance of the low-energy effective Hamiltonian. However, real lattice systems hosting a TI state might have at most a discrete  $n$ -fold rotation symmetry, with  $n = 2, 3, 4, 6$  depending on the lattice point group. Even if the microscopic lattice has this symmetry, the actual device geometry or the presence of disorder might also break it. One might thus wonder to what extent the continuum model results apply to real systems.

The effect of a discrete  $n$ -fold axis is that it enforces angular momentum conservation only modulo  $n$ . This constraint is weaker than that induced by full rotations, but it can still be enough to enforce a gapless superconducting state. Consider the example of the previous section where only the lowest mode is occupied at  $\eta = 1/2$ . Since the angular momentum mismatch between electron and hole state is 1, even a twofold axis (enforcing angular momentum conservation modulo 2) is enough to prevent the mixing of these two bands. If we thread a flux of  $\eta = 3/2$ , electron and hole branches at the Fermi level have angular momentum of  $l = \pm 3/2$ , with a mismatch of 3, and again any twofold axis prevents a gap opening. Notably, however, a threefold axis would not prevent a gap opening in this case, as angular momentum is conserved only modulo 3. The general logic is clear: for an even-fold rotation axis, the lowest energy mode at half-integer flux can never be gapped out by superconductivity without a vortex.

When all relevant symmetries are broken, superconductivity will in general induce a fully gapped state. There remains however the practical matter of how large the gap can be in this case. To illustrate the symmetry constraints and to study the effects of symmetry breaking quantitatively, we now consider a lattice model for a proximitized TI nanowire in several geometries. We consider the model in Ref. [23], with BdG Hamiltonian

$$H_k = [\epsilon - 2t(\cos k_x + \cos k_y + \cos k_z)]\sigma_x\tau_z + \lambda_z\sigma_y\tau_z \sin k_z + \lambda\sigma_z\tau_z(s_y \sin k_x - s_x \sin k_y) + \tau_x\text{Re}\Delta + \tau_y\text{Im}\Delta - \mu\tau_z \quad (20)$$

where  $\sigma, s, \tau$  denote Pauli matrices for orbital, spin and particle-hole degrees of freedom. We take a geometry where the  $x$  and  $y$  directions are finite, extending  $N_x$  and  $N_y$  sites in each direction (note in this section we take a rotated coordinate system where the wire is aligned in the  $z$  direction). We take the parameter values  $t = \lambda = 1$ ,  $\lambda_z = 1.8$  and  $\epsilon = 4$ . Denoting the site number with a discrete pair of indices  $i, j$ , the matrix elements of the Hamiltonian are

$$H_{(i,j),(i,j)} = [\epsilon - 2t \cos k_z]\sigma_x\tau_z + \lambda_z\sigma_y\tau_z \sin k_z + \tau_x\text{Re}\Delta_{i,j} + \tau_y\text{Im}\Delta_{i,j} - \mu\tau_z, \quad (21)$$

$$H_{(i,j),(i+1,j)} = (-t\sigma_x\tau_z + i\lambda/2\sigma_zs_y\tau_z)e^{i\tau_z\phi_j}, \quad (22)$$

$$H_{(i,j),(i,j+1)} = (-t\sigma_x\tau_z - i\lambda/2\sigma_zs_x\tau_z)e^{i\tau_z\phi_i}, \quad (23)$$

where  $\phi_i$  and  $\phi_j$  implement the Peierls phase for constant flux and  $\Delta_{i,j}$  is complex and may contain any number of vortices. This Hamiltonian has particle hole symmetry given by  $U_c H^*(-k) U_c^\dagger = -H(k)$ , with  $U_c = s_y\tau_y$ .

In the absence of pairing this model correctly produces a bulk insulator with a Dirac fermion surface state [24], and its lowest energy modes respond to the flux in the same way as in the effective low energy model, with the caveat that the physical value of the flux that produces a gapless spectrum might deviate somewhat from  $1/2$  due to the penetration depth

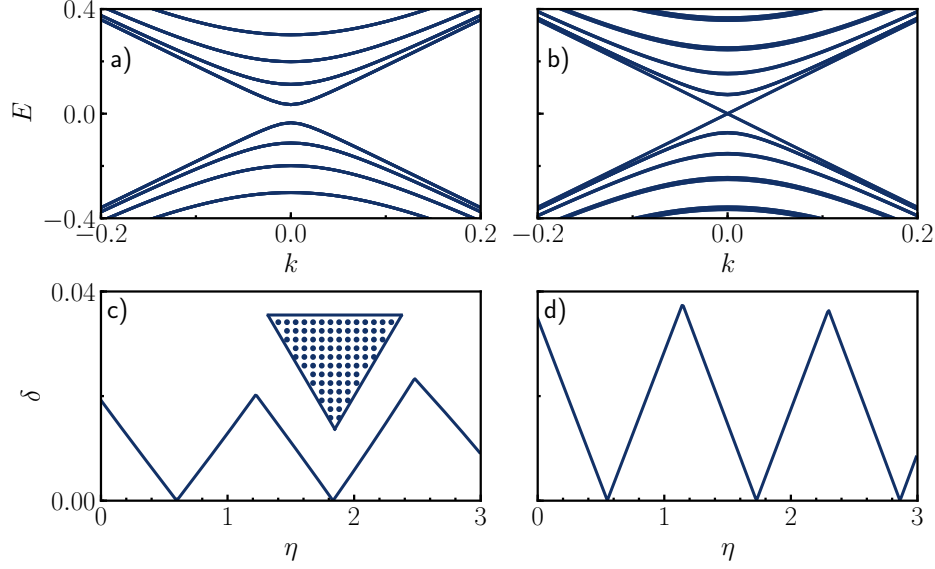


Figure 4: Spectra of the triangular topological insulator nanowire shown in the inset to c), obtained in the tight binding model with  $\Delta = \mu = 0$ , in the presence of magnetic flux at a) zero flux and b)  $\eta = 0.6$  where it becomes gapless. The flux required for closing the gap is larger than 0.5 due to finite size effects. c) Gap as a function of flux for the same triangular wire, showing several zeros. d) Gap as a function of flux for a square wire with  $N_x = N_y = 10$ , showing zeros at different positions due to finite size effects.

of the surface state into the bulk. These finite size effects are also observed in more realistic ab-initio calculations of topological insulator nanowires [41]. As an example illustrating these features, in Figs. 4(a,b) we present the spectrum of a triangular wire with shape depicted in the inset to Fig. 4(c), at  $\eta = 0$  and  $\eta = 0.6$  where the gap closes. The spectrum indeed reproduces that of the effective model. We have chosen this triangular wire as an example with no rotation axis. The same spectrum is obtained for square wires (not shown). Figs. 4(c,d) show the minimum gap between the lowest energy bands at  $k = 0$  for the triangular wire and a square wire for comparison, emphasizing that gap closings occur periodically as in the effective model, but at fluxes that depend on the wire details.

We now produce the same type of phase diagrams as for the continuum model for comparison. To compute the Kitaev number we again need to express  $H$  in the Majorana basis, which is achieved by a unitary transformation  $H^M = UH U^\dagger$ , with  $U$  given by Eq. (10). After this transformation the Hamiltonian is

$$H_k = -[\epsilon - 2t(\cos k_x + \cos k_y + \cos k_z)]\sigma_x\tau_y - \lambda_z\sigma_y\tau_y \sin k_z - \lambda_z\sigma_z s_y\tau_y \sin k_x - \lambda_z\sigma_z s_x \sin k_y + s_y\tau_x \text{Re}\Delta + s_y\tau_z \text{Im}\Delta + \tau_y\mu \quad (24)$$

and the matrix elements are

$$H_{(i,j),(i,j)} = -[\epsilon - 2t \cos k_z]\sigma_x\tau_y - \lambda_z\sigma_y\tau_y \sin k_z + s_y\tau_x \text{Re}\Delta_{i,j} + s_y\tau_z \text{Im}\Delta_{i,j} + \mu\tau_y, \quad (25)$$

$$H_{(i,j),(i+1,j)} = (t\sigma_x\tau_y - i\lambda/2\sigma_z s_y\tau_y)e^{-i\tau_y\phi_j}, \quad (26)$$

$$H_{(i,j),(i,j+1)} = (t\sigma_x\tau_y - i\lambda/2\sigma_z s_x)e^{-i\tau_y\phi_i}. \quad (27)$$

In this basis  $iH$  is a real antisymmetric matrix at  $k = 0, \pi$ , and the Kitaev number is given by Eq. (8).

### 3.1 Phase diagrams

We now consider a number of wire geometries and setups, and present phase diagrams for these showing the topological invariant and the estimate of the gap computed from the transfer matrix as described in the previous section. Fig. 5 shows phase diagrams arranged in the same way as in Fig. 3 for the continuum model, where the left subcolumn of each panel considers pairing without a vortex, while the right subcolumn considers pairing with a vortex. In Fig. 5(a) we consider a square wire with  $N_x = N_y = 10$ , which has fourfold rotation symmetry. We see that the results match almost identically to the continuum model results in Fig. 3 for both subcolumns. Note in particular that in the absence of a vortex, the only gapped states occur around zero flux and are trivial. The presence of a fourfold axis in this case is enough to enforce gaplessness around  $\eta = 1/2$  as in the continuum model, where the topological region was expected. These results are in contrast with a previous lattice calculation of essentially the same geometry [24], which did find some gapped, non-trivial regions.

Considering possible explanations for the discrepancy, in Fig. 5(b) we present the same calculation with a choice of vector potential that is off centered with respect to the fourfold axis  $\vec{A} = B_{\parallel}/2(y - y_0, -(x - x_0), 0)$ . In the absence of pairing, this is just a choice of gauge and makes no difference in the spectrum. However, in the presence of pairing, this has the physical meaning of an inhomogeneous supercurrent profile, which breaks the four-fold axis in a physical way. We observe that in the absence of a vortex, we now get gapped, topological regions around  $\eta = 1/2$ . This reveals the importance of choosing a suitable vector potential, and might be a possible explanation of the discrepancy in the calculations. In practice one only expects an inhomogeneous supercurrent if the wire itself is inhomogeneous.

We next consider disorder, a more physical mechanism that might lead to a topological superconductor without a vortex by breaking rotation symmetries. As the simplest example, we consider a wire with a potential that is constant along the wire, but which fluctuates across the wire cross section. That is, in Eq. (25) we take  $\mu \rightarrow \mu + \delta\mu_{i,j}$  where  $\delta\mu_{i,j}$  is a random number uniformly distributed in the range  $[-W, W]$ . Figs. 5(c,d) show two phase diagrams for two strengths of disorder  $W$ . We see that weak disorder in Fig. 5(c) again enables gapped topological regions in the absence of a vortex, but with a magnitude of the gap that is much smaller than the pairing strength. Strong disorder, shown in Fig. 5(d), allows gapped regions to emerge everywhere in the phase diagram.

We next consider further mechanisms to break the fourfold axis, now only in the absence of a vortex. Fig 6(a) shows the square wire again for reference, while Fig. 6(b) shows a rectangular wire with only a twofold rotation symmetry. In the case of the square wire, the only difference with the continuum model predictions is that a small gap opens at flux near  $\eta = 2$ . In this case, the lowest two degenerate bands have an angular momentum mismatch of 4, so a fourfold axis does not prevent a gapping out of the bands. Similarly, in the case of the rectangular wire, we observe another gapped region around  $\eta = 1$ , where the lowest two degenerate bands have an angular momentum mismatch of 2. These two regions are trivial, but illustrate the effect of different rotation axis in the superconducting state.

Fig. 6(c) shows the same phase diagram for a triangular wire with has no rotation symmetries, where we observe that a very small gap is opened for all values of the flux. Finally, Fig. 6(d) represents a more realistic account of the situation in Fig. 1(b), where the proximity

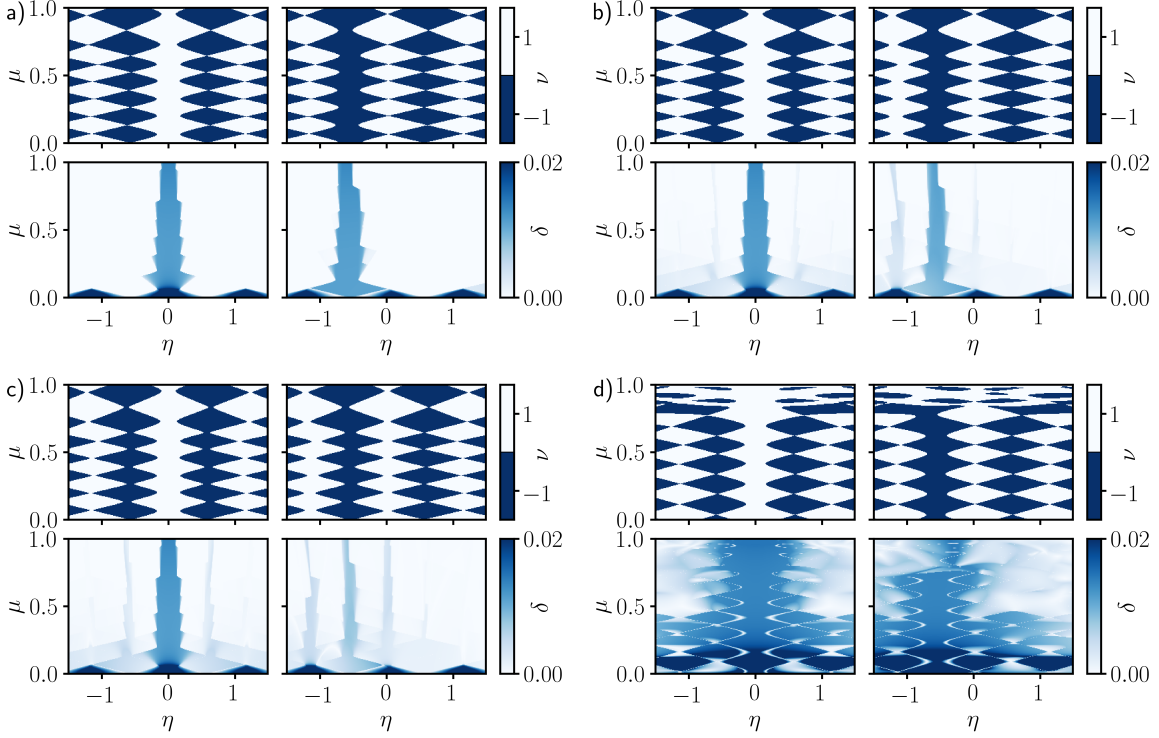


Figure 5: Phase diagram and gap obtained from the tight binding model in the presence of flux and pairing. Subpanels are arranged in the same way as in Fig. 3 where analytical results are shown. a) Results for a clean, square wire with  $N_x = N_y = 10$ . b) Results in the presence of an asymmetric supercurrent profile, which is modeled by choosing the origin of the gauge potential offset from the center of the wire ( $x_0 = 2.25$ ). c) Results for a disordered wire with  $W = 0.1$ . d) Results for a disordered wire with  $W = 0.4$ .

effect is only induced in the few layers closest to the bulk superconductor, and again no symmetries remain. In this case a small gap again opens for every value of the flux. The lowest row of plots show a cut of the estimated gap for a given chemical potential, emphasizing that with no rotation symmetry the gap is always finite but small.

## 4 Discussion and conclusions

The main conclusion to be drawn from this work is that a topological superconducting state can be engineered with topological insulator nanowires in magnetic fields, but the magnitude of the induced superconducting gap is strongly dependent on the device geometry, and in particular on whether there is a superconducting vortex winding around the perimeter of the wire. In the absence of such vortex, discrete rotation symmetries may enforce a gapless state, and if these symmetries are broken only weakly, the gap will be correspondingly very small. We have illustrated this point with an effective model for a TI with  $C_4$  symmetry, by breaking the symmetry in different ways. It is interesting to note that gapless superconductivity

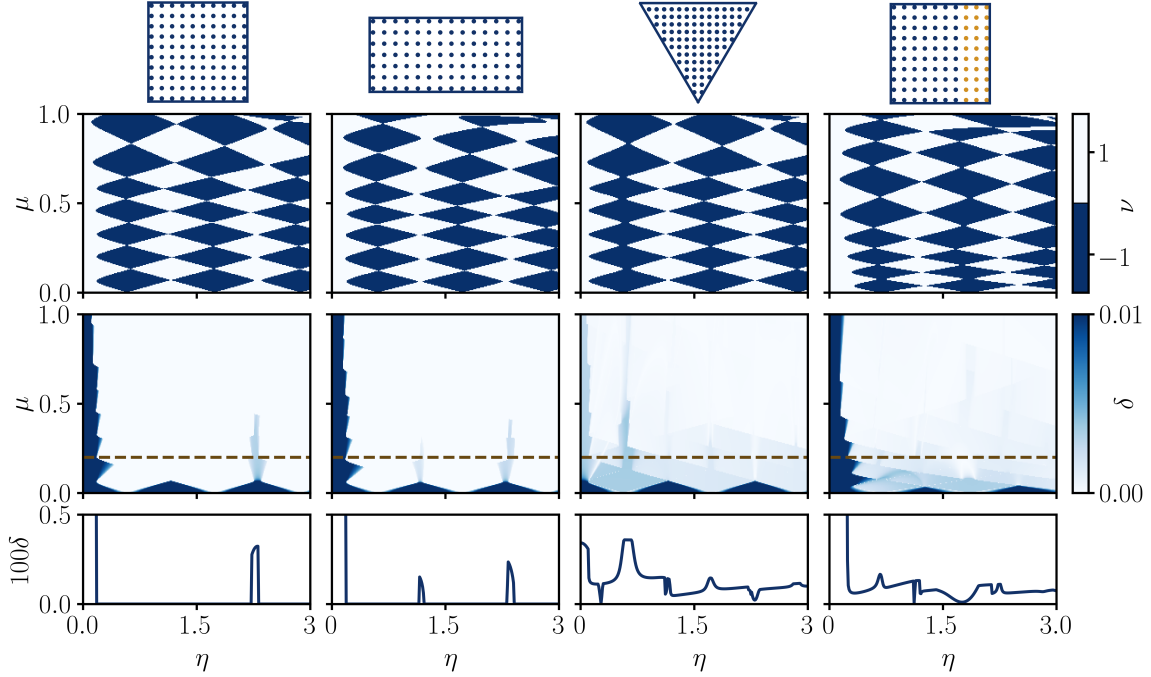


Figure 6: Topological invariant and gap for different ways of breaking the  $C_4$  rotation, in the absence of a vortex in the order parameter. The top row shows the wire geometry: from left to right, the  $C_4$  invariant square wire for reference; a rectangular wire with  $N_x = 10$ ,  $N_y = 7$  and only  $C_2$  rotational symmetry; the triangular wire from Fig. 5, where all symmetries are lost; and a square wire where the proximity effect is finite only for sites with  $N_x > 7$ , representing the situation described in Fig 1. Second row is the Kitaev number, and third row the gap estimate. The fourth row zooms in on the dashed lines in the third row.

has also been predicted in core-shell semiconductor wires with threefold symmetry, which become gapped once this symmetry is broken [42]. These symmetry enforced gapless states are therefore not unique to TIs.

For actual devices made of the prototypical TI  $\text{Bi}_2\text{Se}_3$  [15,43], with point group  $D_{3d}$ , similar conclusions will apply. Wires with well defined facets grown along the crystallographic  $c$  axis will have a threefold symmetry if their cross section is triangular or hexagonal, while wires grown along the  $a$  axis will have twofold symmetry if their cross section is rectangular [15]. This symmetries might be broken depending on the way the superconductor layer is grown. Quantitative predictions for these systems can be made with more realistic  $sp^3$  tight binding models [44,45] and a more microscopic account of the proximity effect as in Ref. [27].

The effect of the Zeeman coupling has not been discussed in this work, as it does not lead to any qualitative changes. The Zeeman coupling to the parallel field can be seen to induce an extra shift of  $\eta$ , which implies that the value of the flux where the perfectly transmitted mode appears further deviates from  $1/2$ . This change occurs in addition to any deviation due to the finite extent of the surface wave functions, as shown in Fig. 4. In any case, the Zeeman  $g$  factor in these systems has been measured to be in the range 6-18 [46]. The Zeeman energy scale for the fields required to make a topological superconductor with this value is of the order of a few meV and its effect is expected to be small.

In a transport experiment, topological superconductivity can be detected via perfect Andreev reflection in a normal-superconductor junction [26], but again it should be noted that this requires a fully gapped state. If the superconductor is gapless, quasiparticle transport contributes in addition to Andreev reflection. A fully gapped state is also required in any proposal that aims at implementing any type of braiding experiments.

In summary, in this work we have presented a detailed account of the influence of an azimuthal vortex in the order parameter of proximitized TI nanowires. We believe that the results presented in this work can serve as a guide to a more realistic implementation of Majorana fermion networks made of topological insulators, and may stimulate further experimental developments.

Note added: While this manuscript was being prepared, an experiment was reported where semiconducting wires were coated with a cylindrical layer of superconductor [47]. Evidence of Majorana fermions was reported, and theoretical account of this result was also reported [48].

## Acknowledgements

The authors would like to thank M. Franz, Y. Chen and Y. Ando for very useful discussions. F. J. was supported by the Marie Curie Programme under EC Grant agreement No. 705968. J. H. B. was supported by the ERC Starting Grant No. 679722 and the Knut and Alice Wallenberg Foundation 2013-0093. This research was supported in part by the National Science Foundation under Grant No. NSF PHY-1748958.

## 5 Appendix

### 5.1 Dirac equation in curved space

In this appendix we review the derivation of the effective Hamiltonian for the surface states of a TI nanowire with an arbitrary cross section, with an emphasis on unifying previous formalisms used for the problem. We consider a surface parametrized by two coordinates  $y^\alpha$  with  $\alpha = 1, 2$ , living in three dimensional space described by coordinates  $x^i$  with  $i = 1, 2, 3$ . Greek indices  $\alpha, \beta, \dots$  will denote surface coordinates, while latin indices  $i, j, \dots$  will denote flat space coordinates. The two basis vectors normal to the surface at every point,  $\vec{e}_1$  and  $\vec{e}_2$ , are given by  $e_\alpha^i = \partial x^i / \partial y^\alpha$ . The unit normal to the surface is  $\vec{n} = \vec{e}_1 \times \vec{e}_2 / |\vec{e}_1 \times \vec{e}_2|$ .

A general effective Hamiltonian valid for any curved surface was first derived in the supplement of Ref. [16]. This is obtained from a 3D massive Dirac fermion model for the bulk by solving for an interface with normal  $\vec{n}$  and then making  $\vec{n}$  position dependent. Setting  $\hbar = v_F = 1$ , the Hamiltonian  $\mathcal{H} = \psi^\dagger H \psi$  is given by

$$H = \frac{\vec{\nabla} \cdot \vec{n}}{2} - \frac{i}{2} \left[ \vec{n} \cdot \vec{\sigma} \times \vec{\nabla} + \vec{\sigma} \times \vec{\nabla} \cdot \vec{n} \right] \quad (28)$$

where  $\vec{\nabla} = (\partial_x, \partial_y, \partial_z)$  and  $\vec{\sigma} = (\sigma_x, \sigma_y, \sigma_z)$ . Since  $\vec{\nabla} \times \vec{n} = 0$ , this can be written as

$$H = \frac{\vec{\nabla} \cdot \vec{n}}{2} - i \vec{n} \cdot \vec{\sigma} \times \vec{\nabla}. \quad (29)$$

This is also the model used in Refs. [23,24]. Since  $\psi$  only depends on the surface coordinates  $y^\alpha$ , the gradient acts as  $\nabla^i \psi = \partial y^\alpha / \partial x^i \partial_\alpha \psi = e_i^\alpha \partial_\alpha \psi$ . The inverse basis vector  $e_i^\alpha \partial_\alpha$  is defined with  $\alpha$  as an upper index by convention. This inverse or conjugate basis satisfies  $\vec{e}^\alpha \vec{e}_\beta = \delta_\beta^\alpha$ . In the Hamiltonian in Eq. 29, the spin is defined with respect to the flat space, constant coordinate system given by  $\hat{x}, \hat{y}, \hat{z}$  as usual. If we were to include the Zeeman coupling with respect to external field, it would take the usual form

$$H = \frac{\vec{\nabla} \cdot \vec{n}}{2} - i\vec{n} \cdot \vec{\sigma} \times \vec{\nabla} + \frac{\mu_B}{2} g \vec{\sigma} \cdot \vec{B}. \quad (30)$$

This Hamiltonian is not written in the standard form of a Dirac Hamiltonian in curved space, which was derived in Ref. [17]. To put it in this form, we can rotate the spin basis by  $\pi/2$  around the normal at each point,  $\psi \rightarrow U\psi$  with  $U = e^{i\frac{\vec{\sigma}\vec{n}}{2}\frac{\pi}{2}} = \frac{1}{\sqrt{2}}(1 + i\vec{\sigma} \cdot \vec{n})$ . The derivative term transforms as

$$-iU^\dagger(\vec{n} \cdot \vec{\nabla} \times \vec{\sigma})U = -i\vec{\sigma} \cdot \vec{\nabla} + \frac{1}{2} \left( -i\vec{\sigma} \cdot \vec{n} \vec{\nabla} \cdot \vec{n} - \vec{\nabla} \cdot \vec{n} \right),$$

where we have used  $2n_i \vec{\nabla} n_i = \vec{\nabla}(\vec{n}^2) = 0$  and  $\vec{\nabla} \times \vec{n} = 0$ . This gives the Hamiltonian

$$H = -i \left( \vec{\sigma} \cdot \vec{\nabla} + \frac{1}{2} \vec{\sigma} \cdot \vec{n} \vec{\nabla} \cdot \vec{n} \right). \quad (31)$$

Remembering that  $\nabla_i \psi = e_i^\mu \partial_\mu \psi$  and defining curved space Dirac matrices  $\alpha^\mu = \vec{e}^\mu \vec{\sigma}$ , Eq. (31) takes the form of a Dirac Hamiltonian in curved space

$$H = -i\alpha^\mu(\partial_\mu + \Gamma_\mu), \quad (32)$$

with

$$\alpha^\mu \Gamma_\mu = \frac{1}{2} \vec{\sigma} \cdot \vec{n} \vec{\nabla} \cdot \vec{n}. \quad (33)$$

This form of the Dirac equation was used in Ref. [17]. There, the spin connection  $\Gamma_\mu$  was defined in terms of the normal Pauli matrix  $\beta = \vec{\sigma} \cdot \vec{n}$  as  $\Gamma_\mu = -\frac{1}{2}\beta\partial_\mu\beta$ . With this definition we have

$$\alpha^\mu \Gamma_\mu = \vec{\sigma} \vec{e}^\mu \left( -\frac{1}{2} \beta \partial_\mu \beta \right) = \frac{1}{2} \beta \vec{\sigma} \vec{e}^\mu \partial_\mu \beta = \frac{1}{2} \beta \vec{\sigma} \vec{\nabla} \beta = \frac{1}{2} \vec{\sigma} \cdot \vec{n} \vec{\nabla} \cdot \vec{n}, \quad (34)$$

which indeed reproduces Eq. (31). If a general Zeeman term had been included, it would have become position dependent due to the rotation  $U$ .

The curved space Dirac Hamiltonian is actually much simpler for a surface that has no intrinsic curvature. For our purposes, we now consider the specific surface of a straight wire, parallel to the  $z$  direction and with arbitrary cross section in the  $x$ - $y$  plane given by the function  $r(\theta)$  (for a cylinder of unit radius we would take  $r(\theta) = 1$ ). Because this surface has no intrinsic (Riemann) curvature, there is a coordinate system where this equation looks like the Dirac equation in flat space, which we now find explicitly. The basis vectors for this surface are

$$\vec{e}_1 = \hat{z}, \quad (35)$$

$$\begin{aligned} \vec{e}_2 &= \frac{\partial x}{\partial \theta} \hat{x} + \frac{\partial y}{\partial \theta} \hat{y} \\ &= (r' \cos \theta - r \sin \theta) \hat{x} + (r' \sin \theta + r \cos \theta) \hat{y}. \end{aligned} \quad (36)$$



With  $r' = \partial_\theta r$ . The conjugate (upper index) basis satisfying  $\vec{e}^i \vec{e}_j = \delta_j^i$  is

$$\vec{e}^1 = \hat{z}, \quad (37)$$

$$\vec{e}^2 = \frac{r' \cos \theta - r \sin \theta}{r'^2 + r^2} \hat{x} + \frac{r' \sin \theta + r \cos \theta}{r'^2 + r^2} \hat{y}. \quad (38)$$

The normal to the surface is

$$\vec{n} = -\frac{(r' \sin \theta + r \cos \theta)}{\sqrt{r'^2 + r^2}} \hat{x} + \frac{(r' \cos \theta - r \sin \theta)}{\sqrt{r'^2 + r^2}} \hat{y}. \quad (39)$$

Defining  $\phi = \arctan r'/r$  we have

$$\alpha^1 = \sigma_z, \quad (40)$$

$$\alpha^2 = \frac{\sin(\phi - \theta)}{\sqrt{r'^2 + r^2}} \sigma_x + \frac{\cos(\phi - \theta)}{\sqrt{r'^2 + r^2}} \sigma_y, \quad (41)$$

and the normal Pauli matrix

$$\beta = \vec{n} \vec{\sigma} = -\cos(\phi - \theta) \sigma_x - \sin(\phi - \theta) \sigma_y. \quad (42)$$

The spin connection is

$$\Gamma_1 = 0, \quad (43)$$

$$\Gamma_2 = -\frac{1}{2} \beta \partial_\theta \beta = \frac{i}{2} (1 - \partial_\theta \phi) \sigma_z. \quad (44)$$

This leaves a final Dirac equation

$$H = -i \left[ \sigma_z \partial_z + \frac{\sin(\phi - \theta) \sigma_x + \cos(\phi - \theta) \sigma_y}{\sqrt{r'^2 + r^2}} (\partial_\theta + \frac{i}{2} (1 - \partial_\theta \phi) \sigma_z) \right]. \quad (45)$$

Now we rotate the Pauli matrices to make them coincide locally with the basis vectors. This is done with the transformation  $\tilde{U} = e^{i\sigma_z(\theta - \phi)/2}$ , which leads to

$$H = -i \left[ \sigma_z \partial_z + \frac{\sigma_y}{\sqrt{r'^2 + r^2}} \partial_\theta \right]. \quad (46)$$

This generalizes the transformation used in Ref. [17] to an arbitrary shape. As this work notes, it is key to realize that  $\tilde{U}$  changes the boundary conditions in  $\theta$  to antiperiodic because  $U(\theta = 2\pi) = -1$ . Finally, we make the coordinate change

$$s = \int_0^\theta d\theta' \sqrt{r'^2(\theta') + r^2(\theta')}, \quad (47)$$

$$\frac{\partial s}{\partial \theta} = \sqrt{r'^2(\theta) + r^2(\theta)}, \quad (48)$$

which indeed leads to the Hamiltonian in the flat space form

$$H = -i [\sigma_z \partial_z + \sigma_y \partial_s]. \quad (49)$$

The coordinate change that brings the equation to flat appearance is an integral equation which in general has no analytic solution except for a few simple cases. But the knowledge of

this coordinate change is not needed unless other position dependent terms are to be included in the Hamiltonian.

This derivation appears to show that if the surface has no intrinsic curvature, then the effective Hamiltonian in an appropriate basis has full rotational invariance in the new variable  $s$ , regardless of the initial cross section. This statement is of course only true to the extent that the linear model is valid. Real wires will only have discrete rotation symmetries, which are apparent when higher order powers or  $k$  are included in the continuum Hamiltonian. The cylindrical model is therefore appropriate only up to the energy cutoff given by the coefficient of the quadratic corrections.

In summary, the effective Hamiltonian for a wire of any cross section takes the form of a standard Dirac Hamiltonian in flat space, with antiperiodic boundary conditions. By making the spin basis rotate to follow the basis vectors, we have introduced an extra  $\pi$  phase that is often described as the "curvature induced" Berry phase. This is the model used in Ref. [26].

## 5.2 Effective Hamiltonian with superconductivity

Given we have presented several different normal Hamiltonians related by local spin rotations, one may wonder whether the formulation of superconductivity still takes its standard form. In this section we spell out the Bogoliubov-de Gennes formulation explicitly to show that this is the case. In second quantized form, an s-wave pairing term takes the form

$$\mathcal{H}_\Delta = \Delta\psi_\uparrow\psi_\downarrow - \Delta^*\psi_\uparrow^*\psi_\downarrow^* = \frac{1}{2} \left[ \Delta\psi^T i\sigma_y \psi - \Delta^*\psi^\dagger i\sigma_y (\psi^\dagger)^T \right], \quad (50)$$

with  $\psi = \begin{pmatrix} \psi_\uparrow \\ \psi_\downarrow \end{pmatrix}$  and  $\psi^\dagger = (\psi_\uparrow^*, \psi_\downarrow^*)$ . This type of term is added to the normal Hamiltonian  $\mathcal{H} = \psi^\dagger H \psi$  to model superconductivity. The different normal Hamiltonians in the previous section are related by spin transformations of the form  $\psi \rightarrow U\psi$  with  $U = e^{i\vec{\sigma}\vec{\alpha}/2}$  where  $\vec{\alpha}$  are position dependent variables. The Hamiltonian for s-wave pairing in Eq. (50) is not affected by such transformations because

$$\begin{aligned} \psi^T i\sigma_y \psi &\rightarrow (U\psi)^T i\sigma_y U\psi = \psi^T e^{i\vec{\sigma}^* \vec{\alpha}/2} i\sigma_y e^{i\vec{\sigma} \vec{\alpha}/2} \psi \\ &= \psi^T i\sigma_y e^{-i\vec{\sigma} \vec{\alpha}/2} e^{i\vec{\sigma} \vec{\alpha}/2} \psi = \psi^T i\sigma_y \psi, \end{aligned}$$

and the same occurs for the complex conjugate term. This is expected since s-wave pairing forms a spin singlet which is rotationally invariant. The total Hamiltonian  $\mathcal{H} + \mathcal{H}_\Delta$  can be rewritten in matrix form in terms of a Nambu spinor  $\Psi = \begin{pmatrix} \psi \\ (\psi^\dagger)^T \end{pmatrix}$  as

$$\mathcal{H} + \mathcal{H}_\Delta = \frac{1}{2} \Psi^\dagger \begin{pmatrix} H & -i\sigma_y \Delta^* \\ i\sigma_y \Delta & -H^T \end{pmatrix} \Psi. \quad (51)$$

This is the BdG formulation used in Refs. [23, 24]. This problem can also be described with an alternative basis where  $\Psi = \begin{pmatrix} \psi \\ -i\sigma_y (\psi^\dagger)^T \end{pmatrix}$  which means the hole operators are time reversed electron operators. In this basis, the Hamiltonian is

$$\mathcal{H} + \mathcal{H}_\Delta = \frac{1}{2} \Psi^\dagger \begin{pmatrix} H & \Delta^* \\ \Delta & -\sigma_y H^* \sigma_y \end{pmatrix} \Psi. \quad (52)$$

This is the formulation used in this work. Both formulations satisfy particle hole symmetry,  $U_C^\dagger H^* U_C = -H$ , with  $U_C = \tau_x$  for the first and  $U = \sigma_y \tau_y$  for the second, where  $\tau$  are Pauli matrices in Nambu space.

### 5.3 Time reversal symmetry in the continuum model

In this work we have used Kitaev's formula to compute topological invariants. A potential caveat for the application of this formula is that this invariant can only be non-trivial when time-reversal symmetry is broken (formally in Hamiltonians of class D [4]). The reason for this is that in a lattice 1D Hamiltonian with spin and time-reversal invariance, there must be Kramers degeneracies at  $k = 0, \pi$ , and the bands must connect these degeneracies such that there are always an even number of Fermi points between  $k = 0$  and  $k = \pi$ . According to Kitaev's criterion, superconductivity must always be of the trivial type when it occurs. The only way to have an odd number of Fermi points with time reversal symmetry in a 1D system is when this is not a bulk 1D system but the 1D boundary of a higher dimensional lattice, as in the well known example of the helical edge state of a 2D topological insulator [49]. In this case, a time-reversal invariant 1D continuum Hamiltonian can be found with a single Fermi point, and superconductivity in this system is indeed topological and features Majorana edge modes.

For topological insulator nanowires, when the applied flux is  $\eta = 0.5$ , or more generally the value that closes the gap, time-reversal symmetry is restored, there is a Kramers degeneracy at  $k = 0$ , and back scattering is forbidden, giving rise to a perfectly transmitted mode [20]. If this is the case, one may wonder how the Kitaev invariant can be non-trivial in the presence of time-reversal symmetry. The reason is the same as in the case of the 2D TI edge: the 1D system under consideration is not a bulk 1D lattice, but the edge of a higher dimensional system.

More explicitly, the continuum model used in this work does indeed have a local effective-time reversal symmetry at  $\eta = 0.5$ . This is also true even in the presence of superconductivity, but only when the vortex is present in the order parameter. One can see this in Eq. (7), reproduced here for clarity, which describes the system in the presence of a vortex after the gauge transformation that removes the winding in the order parameter,

$$H_l^{(1)} = \left[ \sigma_x k + \frac{1}{R} \left( l - \left( \eta - \frac{1}{2} \right) \tau_z \right) \sigma_y - \mu \right] \tau_z + \tau_x \Delta_0. \quad (53)$$

When  $\eta = 0.5$ , this Hamiltonian has the usual time-reversal symmetry  $H = U_T^\dagger H^* U$  with  $U_T = i\sigma_y$  (and  $k, l \rightarrow -k, -l$ ). At  $\Delta = 0$ , there is indeed a Kramers degeneracy at  $k = 0$ . For finite  $\Delta$ , this Hamiltonian realizes a topological superconductor in 1D with time reversal symmetry, as one can see from the Pfaffian corresponding to the  $l = 0$  sector in Eq. (18), which is always negative. This continuum Hamiltonian does not describe a bulk 1D system but rather the surface of a 3D TI, and it is allowed to have a single Fermi point.

### 5.4 Transfer matrix method

Here we describe the method used to compute the estimate for the gap  $\delta$  efficiently. Since we are only interested in states near the Fermi level, we would like to find all values of  $k$  (real or complex) for which there is a solution of

$$[H(k) - \mu] \psi_k = 0. \quad (54)$$

If all solutions to this equation are complex, this means there is no propagating state at the Fermi level and the Hamiltonian is gapped. If a real solution is found, then it is gapless. An efficient way to compute  $k$  numerically is via the transfer matrix  $T$  of the system [50]. The

$T$  matrix of a general 1D tight-binding chain with  $N$  orbitals per site and nearest neighbor hoppings (with lattice constant  $a = 1$ ) is defined as follows. If the Hamiltonian of the chain is

$$H = u + e^{ik}t + e^{-ik}t^\dagger, \quad (55)$$

where  $u$  and  $t$  are  $N \times N$  matrices describing all the on-site and nearest neighbour terms, respectively (and it is assumed that  $t$  is invertible), the transfer matrix at energy  $\epsilon$  is then defined as

$$T = \begin{pmatrix} (t^\dagger)^{-1}(\epsilon - u) & (t^\dagger)^{-1} \\ -t & 0 \end{pmatrix}. \quad (56)$$

An eigenvalue  $\lambda$  of  $T$  with eigenvector  $\psi_\lambda$  satisfies

$$(T - \lambda \mathcal{I})\psi_\lambda = 0 \quad (57)$$

and can be found by solving  $\det(T - \lambda \mathcal{I}) = 0$ . To see the relation with the eigenstates of  $H$ , we multiply Eq. (57) by the following matrix

$$M = \begin{pmatrix} t^\dagger & \lambda^{-1}\mathcal{I} \\ 0 & t^\dagger \end{pmatrix} \quad (58)$$

and obtain

$$M(T - \lambda \mathcal{I})\psi_\lambda = \begin{pmatrix} \epsilon - u - \lambda t^\dagger - \lambda^{-1}t & 0 \\ -t^\dagger t & -\lambda t^\dagger \end{pmatrix} \psi_\lambda = 0. \quad (59)$$

This equation implies that

$$\det(t^\dagger)^2 \det(T - \lambda \mathcal{I}) = \det(\epsilon - u - \lambda t^\dagger - \lambda^{-1}t) \det(-\lambda t^\dagger). \quad (60)$$

Since  $t^\dagger$  is invertible, if  $\lambda$  is an eigenvalue of  $T$  we must have

$$\det(\epsilon - u - \lambda t^\dagger - \lambda^{-1}t) = 0, \quad (61)$$

which is the condition for an eigenvalue of  $H$  if  $\lambda = e^{-ik}$  (with  $k$  real or complex). Therefore, the momenta of all propagating and evanescent modes at energy  $\epsilon$  can be obtained from the transfer matrix eigenvalues as

$$k = i \log \lambda. \quad (62)$$

Moreover, by writing  $\psi_\lambda$  in terms of its block components  $\psi_\lambda = (\psi_{1,\lambda}, \psi_{2,\lambda})^T$ , the first row of Eq. (59) then implies that

$$(\epsilon - u - \lambda t^\dagger - \lambda^{-1}t)\psi_{1,\lambda} = 0 \quad (63)$$

so that  $\psi_{1,\lambda}$  is the eigenvector corresponding to the momentum  $k = i \log \lambda$ .

To apply this method to the tight binding Hamiltonian defined in the main text in Eq. 20, we Fourier transform the  $z$  direction back to real space, where  $\psi_k^\dagger \cos k_z \psi_k \rightarrow \frac{1}{2}(\psi_i^\dagger \psi_{i+1} + \psi_{i+1}^\dagger \psi_i)$  and  $\psi_k^\dagger \sin k_z \psi_k \rightarrow \frac{i}{2}(\psi_i^\dagger \psi_{i+1} - \psi_{i+1}^\dagger \psi_i)$ , where  $i$  denotes the  $i$ -th site along  $z$ . These become hopping terms that enter the matrix  $t$  in Eq. 55.

To apply this method to a continuum Hamiltonian such as the one in Eq. 3, we need to find a lattice Hamiltonian that reproduces the continuum Hamiltonian in the low energy limit. To do this, we simply replace  $\psi_k^\dagger k_z \psi_k \rightarrow \psi_k^\dagger \sin k_z \psi_k$  and then Fourier transform back to real space as before. Note this replacement introduces a second low-energy Dirac fermion at  $k = \pi$  but this poses no problem for our purposes: eigenstates of the continuum model can be obtained from those of  $T$  by selecting those with  $Re[k] \leq \Lambda$  with  $\Lambda$  a momentum cutoff above which the Dirac model is no longer applicable.

## References

- [1] C. Nayak, S. H. Simon, A. Stern, M. Freedman and S. Das Sarma, *Non-abelian anyons and topological quantum computation*, Rev. Mod. Phys. **80**, 1083 (2008), doi:10.1103/RevModPhys.80.1083.
- [2] J. Alicea, *New directions in the pursuit of majorana fermions in solid state systems*, Rep. Prog. Phys. **75**(7), 076501 (2012).
- [3] C. Beenakker, *Search for majorana fermions in superconductors*, Annu. Rev. Con. Mat. Phys. **4**, 113 (2013).
- [4] M. Sato and Y. Ando, *Topological superconductors: a review*, Rep. Prog. Phys. **80**(7), 076501 (2017).
- [5] R. Aguado, *Majorana quasiparticles in condensed matter*, Riv. Nuovo Cim. **40**, 523 (2017).
- [6] Y. Oreg, G. Refael and F. von Oppen, *Helical liquids and majorana bound states in quantum wires*, Phys. Rev. Lett. **105**, 177002 (2010), doi:10.1103/PhysRevLett.105.177002.
- [7] R. M. Lutchyn, J. D. Sau and S. Das Sarma, *Majorana fermions and a topological phase transition in semiconductor-superconductor heterostructures*, Phys. Rev. Lett. **105**, 077001 (2010), doi:10.1103/PhysRevLett.105.077001.
- [8] J. Alicea, Y. Oreg, G. Refael, F. von Oppen and M. P. Fisher, *Non-abelian statistics and topological quantum information processing in 1d wire networks*, Nat. Phys. **7**(5), 412 (2011).
- [9] A. Y. Kitaev, *Unpaired majorana fermions in quantum wires*, Physics-Uspekhi **44**(10S), 131 (2001).
- [10] R. Lutchyn, E. Bakkers, L. Kouwenhoven, P. Krogstrup, C. Marcus and Y. Oreg, *Majorana zero modes in superconductor-semiconductor heterostructures*, Nat. Rev. Mater. p. 1 (2018).
- [11] S. Nadj-Perge, I. K. Drozdov, J. Li, H. Chen, S. Jeon, J. Seo, A. H. MacDonald, B. A. Bernevig and A. Yazdani, *Observation of majorana fermions in ferromagnetic atomic chains on a superconductor*, Science **346**(6209), 602 (2014).
- [12] E. Bocquillon, R. S. Deacon, J. Wiedenmann, P. Leubner, T. M. Klapwijk, C. Brüne, K. Ishibashi, H. Buhmann and L. W. Molenkamp, *Gapless andreev bound states in the quantum spin hall insulator hgte*, Nature Nanotech. **12**(2), 137 (2017).
- [13] V. S. Pribiag, A. J. Beukman, F. Qu, M. C. Cassidy, C. Charpentier, W. Wegscheider and L. P. Kouwenhoven, *Edge-mode superconductivity in a two-dimensional topological insulator*, Nature Nanotech. **10**(7), 593 (2015).
- [14] M. Z. Hasan and C. L. Kane, *Colloquium: topological insulators*, Rev. Mod. Phys. **82**(4), 3045 (2010).

- [15] H. Zhang, C.-X. Liu, X.-L. Qi, X. Dai, Z. Fang and S.-C. Zhang, *Topological insulators in  $bi_2se_3$ ,  $bi_2te_3$  and  $sb_2te_3$  with a single dirac cone on the surface*, Nat. Phys. **5**(6), 438 (2009).
- [16] P. M. Ostrovsky, I. V. Gornyi and A. D. Mirlin, *Interaction-induced criticality in  $z_2$  topological insulators*, Phys. Rev. Lett. **105**, 036803 (2010), doi:10.1103/PhysRevLett.105.036803.
- [17] Y. Zhang and A. Vishwanath, *Anomalous aharonov-bohm conductance oscillations from topological insulator surface states*, Phys. Rev. Lett. **105**(20), 206601 (2010).
- [18] J. H. Bardarson, P. W. Brouwer and J. E. Moore, *Aharonov-bohm oscillations in disordered topological insulator nanowires*, Phys. Rev. Lett. **105**(15), 156803 (2010).
- [19] R. Egger, A. Zazunov and A. L. Yeyati, *Helical luttinger liquid in topological insulator nanowires*, Phys. Rev. Lett. **105**, 136403 (2010), doi:10.1103/PhysRevLett.105.136403.
- [20] J. H. Bardarson and J. E. Moore, *Quantum interference and aharonov-bohm oscillations in topological insulators*, Rep. Prog. Phys. **76**(5), 056501 (2013).
- [21] E. Xypakis, J.-W. Rhim, J. H. Bardarson and R. Ilan, *Perfect transmission in rippled topological insulator nanowires*, arXiv:1712.06478 (2017).
- [22] K. Moors, P. Schüffelgen, D. Rosenbach, T. Schmitt, T. Schäpers and T. L. Schmidt, *Magnetotransport signatures of 3d topological insulator nanowire structures*, arXiv:1801.09230 (2018).
- [23] A. Cook and M. Franz, *Majorana fermions in a topological-insulator nanowire proximity-coupled to an s-wave superconductor*, Phys. Rev. B **84**, 201105 (2011), doi:10.1103/PhysRevB.84.201105.
- [24] A. M. Cook, M. M. Vazifeh and M. Franz, *Stability of majorana fermions in proximity-coupled topological insulator nanowires*, Phys. Rev. B **86**, 155431 (2012), doi:10.1103/PhysRevB.86.155431.
- [25] R. Ilan, J. H. Bardarson, H.-S. Sim and J. E. Moore, *Detecting perfect transmission in Josephson junctions on the surface of three dimensional topological insulators*, New J. Phys. **16**(5), 053007 (2014).
- [26] F. de Juan, R. Ilan and J. H. Bardarson, *Robust transport signatures of topological superconductivity in topological insulator nanowires*, Phys. Rev. Lett. **113**, 107003 (2014), doi:10.1103/PhysRevLett.113.107003.
- [27] P. Sitthison and T. D. Stanescu, *Robustness of topological superconductivity in proximity-coupled topological insulator nanoribbons*, Phys. Rev. B **90**, 035313 (2014), doi:10.1103/PhysRevB.90.035313.
- [28] G.-Y. Huang and H. Q. Xu, *Majorana fermions in topological-insulator nanowires: From single superconducting nanowires to josephson junctions*, Phys. Rev. B **95**, 155420 (2017), doi:10.1103/PhysRevB.95.155420.

- [29] J. Manousakis, A. Altland, D. Bagrets, R. Egger and Y. Ando, *Majorana qubits in a topological insulator nanoribbon architecture*, Phys. Rev. B **95**, 165424 (2017), doi:10.1103/PhysRevB.95.165424.
- [30] J. Dufouleur, L. Veyrat, A. Teichgräber, S. Neuhaus, C. Nowka, S. Hampel, J. Cayssol, J. Schumann, B. Eichler, O. G. Schmidt, B. Büchner and R. Giraud, *Quasiballistic transport of dirac fermions in a  $\text{Bi}_2\text{Se}_3$  nanowire*, Phys. Rev. Lett. **110**, 186806 (2013), doi:10.1103/PhysRevLett.110.186806.
- [31] S. S. Hong, Y. Zhang, J. J. Cha, X.-L. Qi and Y. Cui, *One-dimensional helical transport in topological insulator nanowire interferometers*, Nano Lett. **14**(5), 2815 (2014).
- [32] S. Cho, B. Dellabetta, R. Zhong, J. Schneeloch, T. Liu, G. Gu, M. J. Gilbert and N. Mason, *Aharonov-bohm oscillations in a quasi-ballistic three-dimensional topological insulator nanowire*, Nat. Commun. **6**, 7634 (2015).
- [33] L. A. Jauregui, M. T. Pettes, L. P. Rokhinson, L. Shi and Y. P. Chen, *Gate tunable relativistic mass and berry's phase in topological insulator nanoribbon field effect devices*, Sci. Rep. **5**, 8452 (2015).
- [34] L. A. Jauregui, M. T. Pettes, L. P. Rokhinson, L. Shi and Y. P. Chen, *Magnetic field-induced helical mode and topological transitions in a topological insulator nanoribbon*, Nat. Nanotech. **11**, 345 (2016).
- [35] J. Kim, A. Hwang, S.-H. Lee, S.-H. Jhi, S. Lee, Y. C. Park, S.-i. Kim, H.-S. Kim, Y.-J. Doh, J. Kim *et al.*, *Quantum electronic transport of topological surface states in  $\beta\text{-ag}_2\text{se}$  nanowire*, ACS Nano **10**(4), 3936 (2016).
- [36] J. Dufouleur, L. Veyrat, B. Dassonneville, E. Xypakis, J. H. Bardarson, C. Nowka, S. Hampel, J. Schumann, B. Eichler, O. Schmidt *et al.*, *Weakly-coupled quasi-1d helical modes in disordered 3d topological insulator quantum wires*, Sci. Rep. **7**, 45276 (2017).
- [37] J. Ziegler, R. Kozlovsky, C. Gorini, M.-H. Liu, S. Weishäupl, H. Maier, R. Fischer, D. A. Kozlov, Z. D. Kvon, N. Mikhailov, S. A. Dvoretzky, K. Richter *et al.*, *Probing spin helical surface states in topological hgte nanowires*, Phys. Rev. B **97**, 035157 (2018), doi:10.1103/PhysRevB.97.035157.
- [38] J. Kim, B.-K. Kim, H.-S. Kim, A. Hwang, B. Kim and Y.-J. Doh, *Macroscopic quantum tunneling in superconducting junctions of  $\beta\text{-ag}_2\text{se}$  topological insulator nanowire*, cond-mat/1708.06041 (2017).
- [39] L. A. Jauregui, M. Kayyalha, A. Kazakov, I. Miotkowski, L. P. Rokhinson and Y. P. Chen, *Gate-tunable supercurrent and multiple andreev reflections in a superconductor-topological insulator nanoribbon-superconductor hybrid device*, Appl. Phys. Lett. **112**(9), 093105 (2018).
- [40] M. Kayyalha, M. Kargarian, A. Kazakov, I. Miotkowski, V. M. Galitski, V. M. Yakovenko, L. P. Rokhinson and Y. P. Chen, *Anomalous low-temperature enhancement of supercurrent in topological-insulator nanoribbon josephson junctions: evidence for low-energy andreev bound states*, arXiv preprint arXiv:1712.02748 (2017).



- [41] F. W. Chen, L. A. Jauregui, Y. Tan, M. Manfra, G. Klimeck, Y. P. Chen and T. Kubis, *In-surface confinement of topological insulator nanowire surface states*, Appl. Phys. Lett. **107**(12), 121605 (2015).
- [42] T. D. Stanescu, A. Sitek and A. Manolescu, *Robust topological phase in proximitized core-shell nanowires coupled to multiple superconductors*, Beilstein J. Nanotechnol. **9**, 1512 (2018).
- [43] C.-X. Liu, X.-L. Qi, H. Zhang, X. Dai, Z. Fang and S.-C. Zhang, *Model hamiltonian for topological insulators*, Phys. Rev. B **82**(4), 045122 (2010).
- [44] A. Pertsova and C. M. Canali, *Probing the wavefunction of the surface states in  $bi_2se_3$  topological insulator: a realistic tight-binding approach*, New J. Phys. **16**(6), 063022 (2014).
- [45] N. Virk, G. Autès and O. V. Yazyev, *Electronic properties of one-dimensional nanostructures of the  $bi_2se_3$  topological insulator*, Phys. Rev. B **97**, 165411 (2018), doi:10.1103/PhysRevB.97.165411.
- [46] Y.-S. Fu, T. Hanaguri, K. Igarashi, M. Kawamura, M. Bahramy and T. Sasagawa, *Observation of zeeman effect in topological surface state with distinct material dependence*, Nature Commun. **7**, 10829 (2016).
- [47] S. Vaitiekėnas, M.-T. Deng, P. Krogstrup and C. Marcus, *Flux-induced majorana modes in full-shell nanowires*, arXiv:1809.05513 (2018).
- [48] R. M. Lutchyn, G. W. Winkler, B. van Heck, T. Karzig, K. Flensberg, L. I. Glazman and C. Nayak, *Topological superconductivity in full shell proximitized nanowires*, arXiv:1809.05512 (2018).
- [49] C. L. Kane and E. J. Mele,  *$Z_2$  topological order and the quantum spin hall effect*, Phys. Rev. Lett. **95**, 146802 (2005), doi:10.1103/PhysRevLett.95.146802.
- [50] A. Umerski, *Closed-form solutions to surface green's functions*, Phys. Rev. B **55**, 5266 (1997), doi:10.1103/PhysRevB.55.5266.